Supporting information for the work entitled

Coalescence of cluster beam generated sub-2 nm bare Au nanoparticles and analysis of Au film growth parameters

Emanuele Verrelli[1,2,*], *Irini Michelakaki*[1], *Nikos Boukos*[3], *Georgios Kyriakou*[4,5], *Dimitris Tsoukalas*[1]

[1]Department of Applied Physics, National Technical University of Athens, Heroon Politechniou 9, Zographou (Athens), 15780, Greece.
[2]Department of Physics and Mathematics, University of Hull, Cottingham road, HU67RX, Kingston upon Hull, United Kingdom.
[3]Institute of Nanoscience and Nanotechnology, National Centre for Scientific Research Demokritos, Terma Patriarchou Grigoriou, Aghia Paraskevi, 15310, Greece
[4]European Bioenergy Research Institute, Aston University, Aston Triangle, Birmingham B4 7ET, United Kingdom.
[5] Chemical Engineering and Applied Chemistry, School of Engineering and Applied Sciences, Aston University, Aston Triangle, Birmingham, B4 7ET, UK.

*Corresponding author. E-mail: verrelli@central.ntua.gr

Contents

1 3D growth vs 2D lateral growth kinetics: theoretical derivation

In this section we will discuss the theoretical implications related with assuming either a 3D growth model or a 2D lateral growth one which in other words is equivalent to assuming that at any stage of the film growth the NPs are always either spherical or disk-like. Given an initial monodisperse NP population of N NPs, in the following paragraphs we will consider idealized situations in which one of the two types of growth is analyzed in stepwise fashion allowing only one process (1-0, 1-1, 1-2, etc) to take place. At every step the diameter and density of the monodisperse NPs will be calculated which then will allow us to determine the corresponding equivalent film thickness and film coverage using the following relations (note that the equation for the coverage is exact under the assumption that NPs don't overlap i.e. the density is such that NPs form less than a complete monolayer):

$$\begin{aligned} thickness &= \sigma \times \langle Vol(NP) \rangle = \frac{\pi}{6} \times \sigma \times D^3, 3Dgrowth \\ thickness &= \sigma \times \langle Vol(NP) \rangle = \frac{\pi}{4} \times \sigma \times h \times D^2, 2Dgrowth \end{aligned} \quad \text{(S1)}$$

$$\text{cov}erage = \sigma \times \langle Area(NP) \rangle = \frac{\pi}{4} \times \sigma \times D^2 \quad \text{(S2)}$$

Let us assume that for all situations analyzed here below the starting assumption is that the cluster beam generates NPs with diameter D_0 and that N NPs are already deposited on our substrate with areal density σ_0.

1.1 3D growth

1.1.1 1-0 processes

Under the assumption of 3D growth, the NPs are spherical at any stage. Assuming that only 1-0 processes take place then as N NPs are deposited on the substrate, 2N NPs will subsequently be on the substrate and we have the following situation:

$$\begin{cases} D_1 = D_0 \\ \sigma_1 = 2 \times \sigma_0 \\ thickness_1 = 2 \times \sigma_0 \times (D_0)^3 = thickness_0 \times 2 \\ \mathrm{cov}erage_1 = 2 \times \sigma_0 \times (D_0)^2 = \mathrm{cov}erage_0 \times 2 \end{cases} \quad \text{(S3)}$$

which at the n-th step would read

$$\begin{cases} D_n = D_0 \\ \sigma_n = (n+1) \times \sigma_0 \\ thickness_n = thickness_0 \times (n+1) \\ \mathrm{cov}erage_n = \mathrm{cov}erage_0 \times (n+1) \end{cases} \quad \text{(S4)}$$

The above parametric equation provides, through few substitutions, the relation between diameter/density/coverage with the thickness of the film. For 1-0 processes it seems that the diameter is constant while density and coverage are linear functions of the film thickness, as someone would expect.

1.1.2 1-1 processes

Assuming that only 1-1 processes take place, N NPs must be deposited in order to interact with the N ones on the substrate and the resulting N NPs on the substrate would have

$$\begin{cases} D_1 = D_0 \times 2^{\frac{1}{3}} \\ \sigma_1 = \sigma_0 \\ thickness_1 = thickness_0 \times 2 \\ \mathrm{cov}erage_1 = \mathrm{cov}erage_0 \times 2 \end{cases} \quad \text{(S5)}$$

which at the n-th step would read

$$\begin{cases} D_n = D_0 \times (n+1)^{\frac{1}{3}} \\ \sigma_n = \sigma_0 \\ thickness_n = thickness_0 \times (n+1) \\ \mathrm{cov}\,erage_n = \mathrm{cov}\,erage_0 \times (n+1)^{\frac{2}{3}} \end{cases} \quad \text{(S6)}$$

1.1.3 1-2 processes

Assuming that only 1-2 process take place, N/2 NPs must be deposited in order to interact with the N ones on the substrate and the resulting N/2 NPs on the substrate would have

$$\begin{cases} D_1 = D_0 \times 3^{\frac{1}{3}} \\ \sigma_1 = \dfrac{\sigma_0}{2} \\ thickness_1 = thickness_0 \times \dfrac{3}{2} \\ \mathrm{cov}\,erage_1 = \mathrm{cov}\,erage_0 \times \dfrac{3^{\frac{2}{3}}}{2} \end{cases} \quad \text{(S7)}$$

which at the n-th step would read

$$\begin{cases} D_n = D_0 \times \left(2^{n+1}-1\right)^{\frac{1}{3}} \\ \sigma_n = \dfrac{\sigma_0}{2^n} \\ thickness_n = thickness_0 \times \dfrac{\left(2^{n+1}-1\right)}{2^n} \\ \mathrm{cov}\,erage_n = \mathrm{cov}\,erage_0 \times \dfrac{\left(2^{n+1}-1\right)^{\frac{2}{3}}}{2^n} \end{cases} \quad \text{(S8)}$$

1.1.4 1-3 processes

Assuming that only 1-3 process take place, N/3 NPs must be deposited in order to interact with the N ones on the substrate and the resulting N/3 NPs on the substrate would have

$$\begin{cases} D_1 = D_0 \times 4^{\frac{1}{3}} \\ \sigma_1 = \dfrac{\sigma_0}{3} \\ thickness_1 = thickness_0 \times \dfrac{4}{3} \\ \mathrm{cov}\,erage_1 = \mathrm{cov}\,erage_0 \times \dfrac{4^{\frac{2}{3}}}{3} \end{cases} \tag{S9}$$

which at the n-th step would read

$$\begin{cases} D_n = D_0 \times \left(\dfrac{3^{n+1}-1}{2}\right)^{\frac{1}{3}} \\ \sigma_n = \dfrac{\sigma_0}{3^n} \\ thickness_n = thickness_0 \times \left(\dfrac{3^{n+1}-1}{2\times 3^n}\right) \\ \mathrm{cov}\,erage_n = \mathrm{cov}\,erage_0 \times \dfrac{1}{3^n} \times \left(\dfrac{3^{n+1}-1}{2}\right)^{\frac{2}{3}} \end{cases} \tag{S10}$$

1.2 2D lateral growth

1.2.1 1-0 processes

Under the assumption of 2D lateral growth, the NPs are disk-like with height h at any step and assuming that only 1-0 processes take place then as N NPs are deposited on the substrate, 2N NPs will subsequently be on the substrate and we have the following situation:

$$\begin{cases} D_1 = D_0 \\ \sigma_1 = 2 \times \sigma_0 \\ thickness_1 = 2 \times \sigma_0 \times h \times \left(D_0\right)^2 = thickness_0 \times 2 \\ \mathrm{cov}\,erage_1 = 2 \times \sigma_0 \times \left(D_0\right)^2 = \mathrm{cov}\,erage_0 \times 2 \end{cases} \tag{S11}$$

which at the n-th step would read

$$\begin{cases} D_n = D_0 \\ \sigma_n = (n+1)\times\sigma_0 \\ thickness_n = thickness_0 \times (n+1) \\ \mathrm{cov}\,erage_n = \mathrm{cov}\,erage_0 \times (n+1) \end{cases} \quad \text{(S12)}$$

The above parametric equation provides, through few substitutions, the relation between diameter/density/coverage with the thickness of the film. For 1-0 processes it seems that the diameter is constant while density and coverage are linear functions of the film thickness, as someone would expect.

1.2.2 1-1 processes

Assuming that only 1-1 process take place, N NPs must be deposited in order to interact with the N ones on the substrate and the resulting N NPs on the substrate would have

$$\begin{cases} D_1 = D_0 \times 2^{\frac{1}{2}} \\ \sigma_1 = \sigma_0 \\ thickness_1 = thickness_0 \times 2 \\ \mathrm{cov}\,erage_1 = \mathrm{cov}\,erage_0 \times 2 \end{cases} \quad \text{(S13)}$$

which at the n-th step would read

$$\begin{cases} D_n = D_0 \times (n+1)^{\frac{1}{2}} \\ \sigma_n = \sigma_0 \\ thickness_n = thickness_0 \times (n+1) \\ \mathrm{cov}\,erage_n = \mathrm{cov}\,erage_0 \times (n+1) \end{cases} \quad \text{(S14)}$$

1.2.3 1-2 processes

Assuming that only 1-2 process take place, N/2 NPs must be deposited in order to interact with the N ones on the substrate and the resulting N/2 NPs on the substrate would have

$$\begin{cases} D_1 = D_0 \times 3^{\frac{1}{2}} \\ \sigma_1 = \dfrac{\sigma_0}{2} \\ thickness_1 = thickness_0 \times \dfrac{3}{2} \\ \mathrm{cov}\,erage_1 = \mathrm{cov}\,erage_0 \times \dfrac{3}{2} \end{cases} \tag{S15}$$

which at the n-th step would read

$$\begin{cases} D_n = D_0 \times \left(2^{n+1} - 1\right)^{\frac{1}{2}} \\ \sigma_n = \dfrac{\sigma_0}{2^n} \\ thickness_n = thickness_0 \times \dfrac{\left(2^{n+1} - 1\right)}{2^n} \\ \mathrm{cov}\,erage_n = \mathrm{cov}\,erage_0 \times \dfrac{\left(2^{n+1} - 1\right)}{2^n} \end{cases} \tag{S16}$$

1.2.4 1-3 processes

Assuming that only 1-3 process take place, N/3 NPs must be deposited in order to interact with the N ones on the substrate and the resulting N/3 NPs on the substrate would have

$$\begin{cases} D_1 = D_0 \times 4^{\frac{1}{2}} \\ \sigma_1 = \dfrac{\sigma_0}{3} \\ thickness_1 = thickness_0 \times \dfrac{4}{3} \\ \mathrm{cov}\,erage_1 = \mathrm{cov}\,erage_0 \times \dfrac{4}{3} \end{cases} \tag{S17}$$

which at the n-th step would read

$$\begin{cases} D_n = D_0 \times \left(\dfrac{3^{n+1}-1}{2} \right)^{\frac{1}{2}} \\ \sigma_n = \dfrac{\sigma_0}{3^n} \\ thickness_n = thickness_0 \times \left(\dfrac{3^{n+1}-1}{2 \times 3^n} \right) \\ \mathrm{cov}erage_n = \mathrm{cov}erage_0 \times \left(\dfrac{3^{n+1}-1}{2 \times 3^n} \right) \end{cases} \qquad \text{(S18)}$$

1.3 Graphical solution of parametric growth equations

The above parametric equations have been solved graphically as shown in Figure S 1 here below.

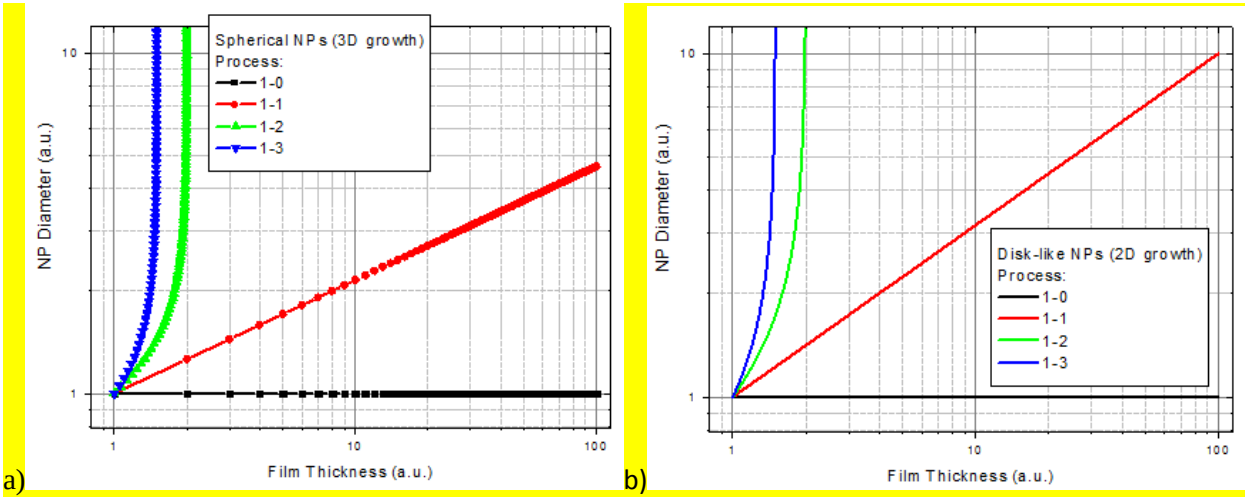

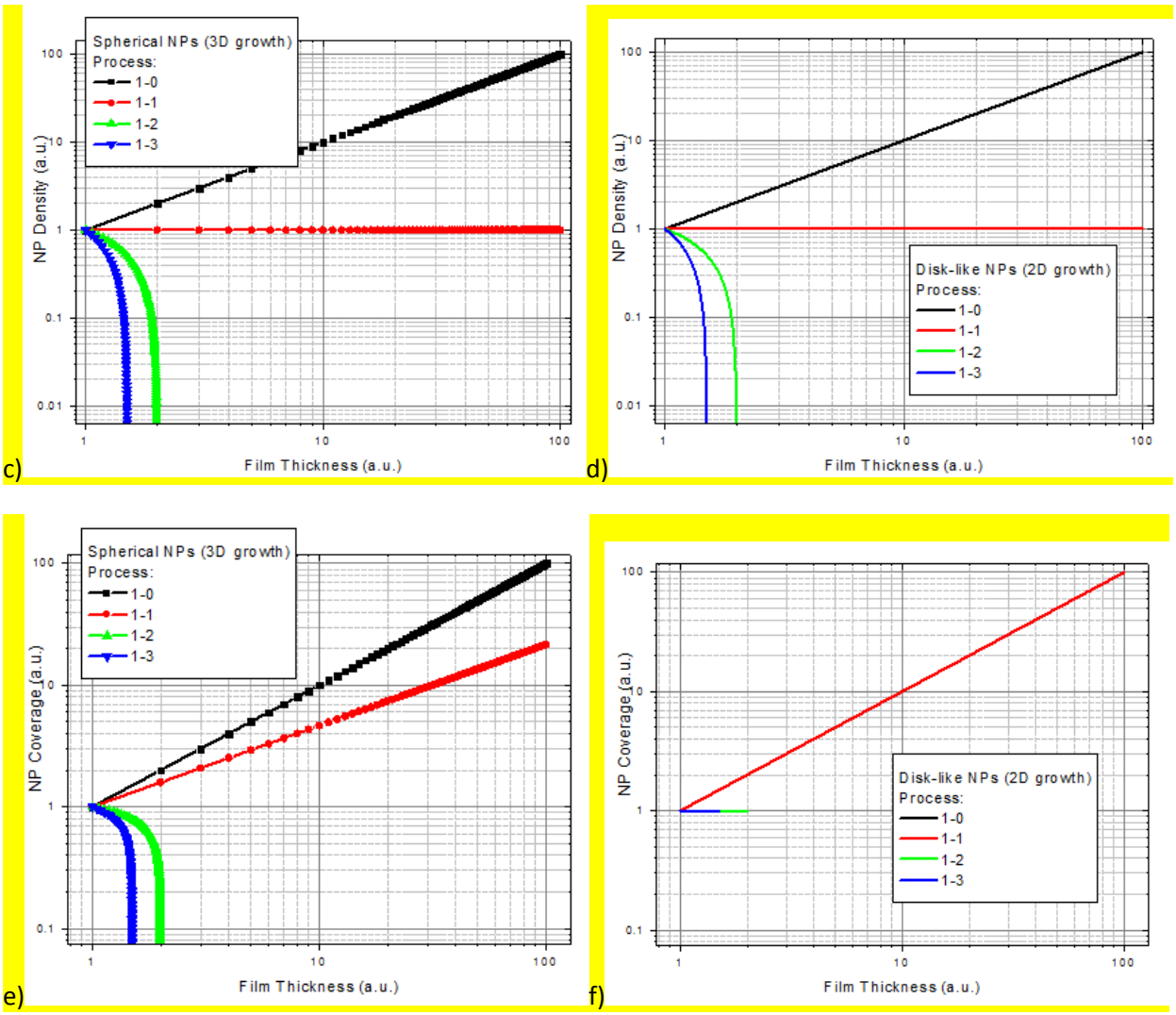

Figure S 1. Theoretical evolution of macroscopic NP film parameters (NP diameter, NP density and NP coverage)as a function of the NP film thickness (according to the parametric equations mentioned in the text) under the assumption of either 3D growth (a, c, e) or 2D lateral growth (b, d, f) and considering the presence of just one coalescence process between NPs (1-0, 1-1, 1-2, etc). Note that all constants and parameters have been replaced with 1 in these graphs.

2 Nearest Neighbor analysis

In Figure S 2 is presented the dependence upon the load of the average nearest neighbor distance (NN), calculated as center-to-center or edge-to-edge, obtained analyzing the TEM images of samples A-D with the GIAS software [1] and Wolfram Mathematica. It is interesting how also in this graph it is possible to distinguish between two clear growth regimes: during landing (up to B) the NN distance decreases while during coalescence (B-D) the NN distance slightly increases. It is quite interesting to note that at the onset of the coalescence regime (B), the NN shows a minimum in a similar fashion to Pedersen et al [2], who observed that below a certain NN limit cluster beam fabricated Ag NPs are seen to naturally coalesce, and could thus represent the evidence that something similar holds also for Au NPs.

2.1 Fine structure of the nearest neighbor distributions

Comparing the NN distributions shown in Figure S 3 it becomes clear that the NN distribution of sample B is not only the one with smallest mean NN distance but is also the one with smallest dispersion which is in agreement with the fact that this sample has highest NP density of all. It is also interesting to note here that as the NP density decreases as we go from sample B to D, which someone could expect to cause the NN distributions to shift to higher values to the right, the peak of the NN distributions is actually always at 1.1 nm while it is the amount of NPs in the tail of the distributions that increases (e.g. NPs with NN >2 nm) causing the slight increase in the mean NN value compared to that of sample B, as shown in Figure S 2.

2.2 Correlation between nearest neighbor distance and NP size

The correlation plots shown in Figure S 3 are meant to highlight any possible correlation existing between the NN distance and the diameter of the NP considered. Some NPs posses NN distances as small as 0.4 nm and it seems that larger NPs are capable of approaching closer to

other NPs than what smaller ones can do. By linear fitting the data we actually discovered 1) a positive but compatible with 0 correlation slope in sample A and B, 2) a negative but compatible with 0 correlation slope in sample C, 3) a negative correlation slope in sample D). Results are summarized in Figure S 4. The above, although very approximate, is suggesting that as the load is increased and thus the NP population changes, the correlation between NN and NP diameter is also affected. From sample A to sample C, which have NP diameter < 5 nm, the NN seem quite independent from the diameter of the corresponding NP. On the other hand for sample D, which has NPs with diameter up to nearly 10 nm, a clear dependence starts showing up with the mean NN getting smaller as the NP diameter considered is increased. This seems supporting the idea that large NPs have mean NN distance smaller than the NN distance of smaller NPs.

Further insight into this matter is provided by the data shown in Figure S 5 and Figure S 6. Here we present analyses of the correlation data "NP diameter vs NN NP diameter" of the 4 samples A-D, performed by dividing the NP population in two groups: the first one made up of those NPs having NN NP with diameter within 20% of its own (blue), and the second one, of those NPs not fulfilling the above condition (purple). In other words, in the first group fall those NPs that have very similar diameter to their NN NP, in the second group are those NPs that have very different diameter from their NN NP. It is quite enlighting the result presented in the summary shown in Figure S 6. NPs in group one have mean NN that decreases from sample A to B and then stays surprisingly constant up to D. On the other hand NPs in group two have mean NN that decreases from A to B and then increases from B to D. the above results support the idea that when NPs have very similar diameters they can stay closer than in any other condition and thus that the driving force causing the coalescence between neighboring NPs (coalescence regime, sample B-D) could be size-difference related. Although the difference between the NN

data in the two groups isn't very big, it is very consistent and is reproduced also for cutoff limits bigger than 20% (e.g. 50%). This result clearly demonstrates that the increasing mean NN values observed in Figure S 2 when moving from sample B toward D can actually be ascribed to those NP belonging to group two mentioned above.

Summarizing, the analysis here presented has highlighted two interesting results that could pinpoint the origin of the kinetic properties of Au NPs of different sizes: 1) large NPs are more likely to have NN distance smaller than the NN distance of small NPs, 2) NPs with diameters very similar to the diameter of the corresponding NN NP have the smallest NN distance. These two results qualitatively agree with the spontaneous charge transfer mechanism mentioned by Pedersen et al. [2].

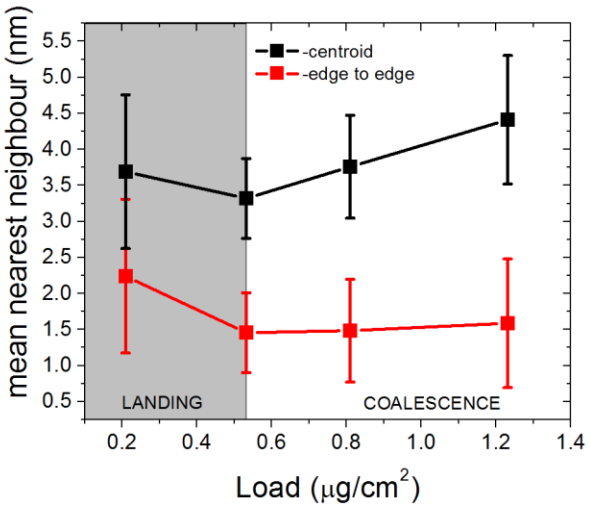

Figure S 2. the mean nearest neighbor distance (NN) as a function of the load. The NN calculated center-to-center is obviously larger than the one calculated as edge-to-edge. The error bars represent twice the standard deviation of the NN distribution. During the landing phase, NN is found to decrease and the NPs density to increase while during the coalescence phase NN increases and the NPs density decreases.

a1)

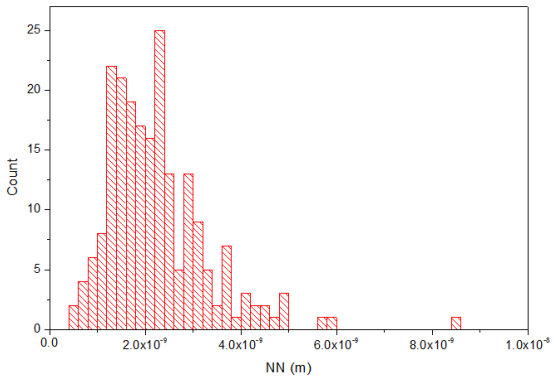

a2)

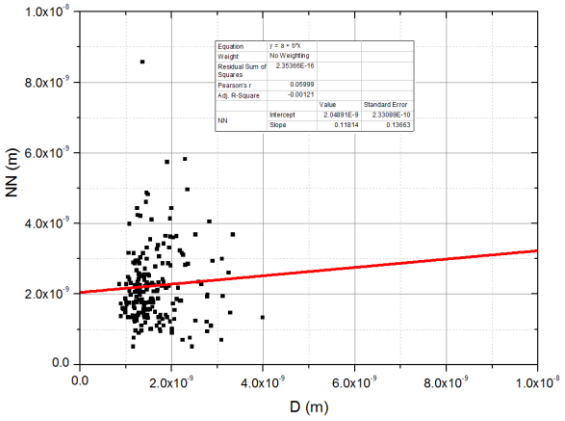

b1)

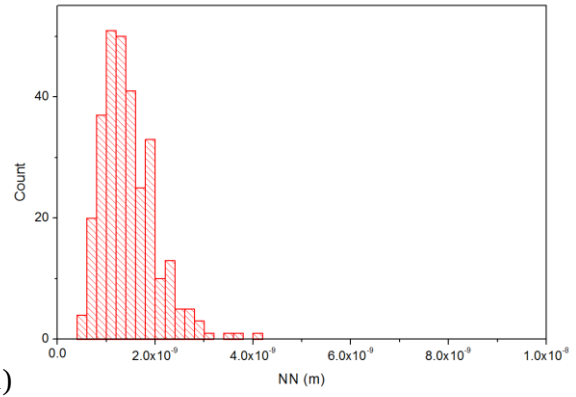

b2)

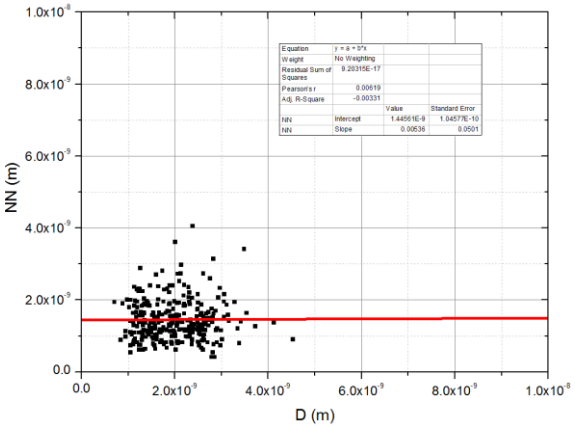

c1)

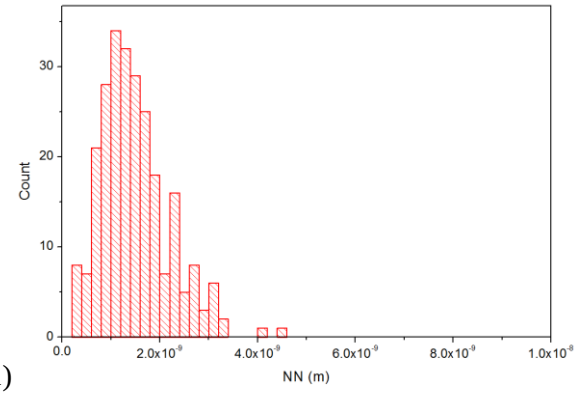

c2)

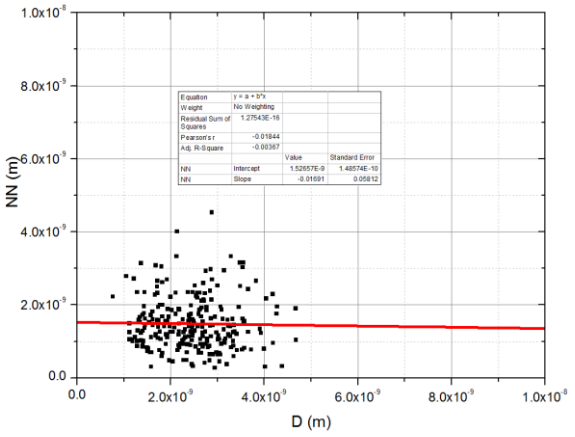

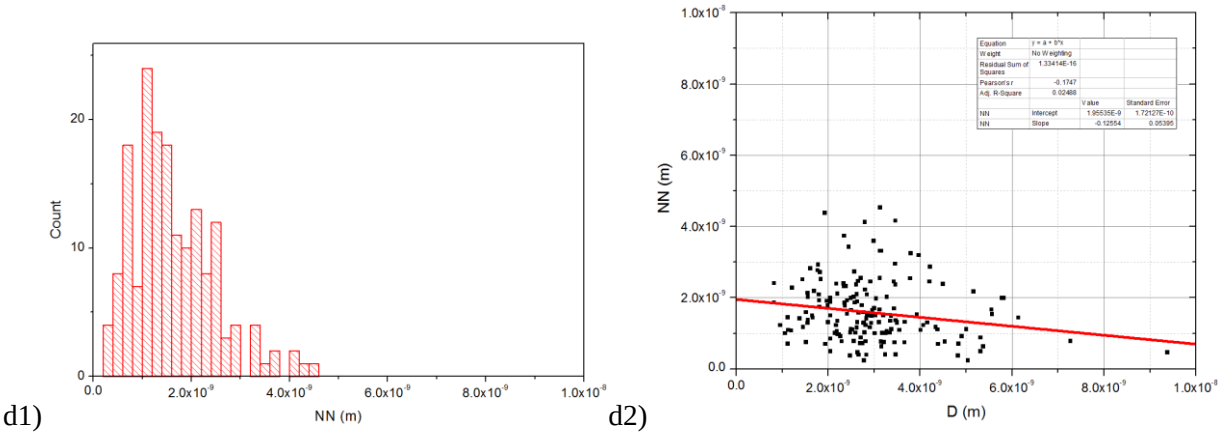

d1) d2)

Figure S 3. a1)-d1) NN distribution for sample A-D. a2)-d2) NN vs NP diameter, correlation plot for sample A-D.

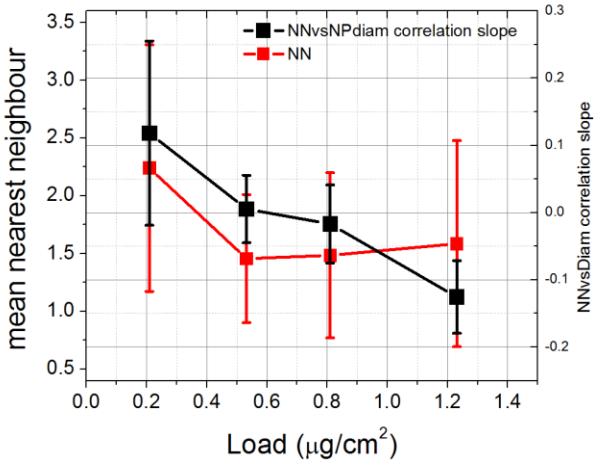

Figure S 4. comparison between the NN and the correlation slope extracted from Figure S 3, as function of the NP load.

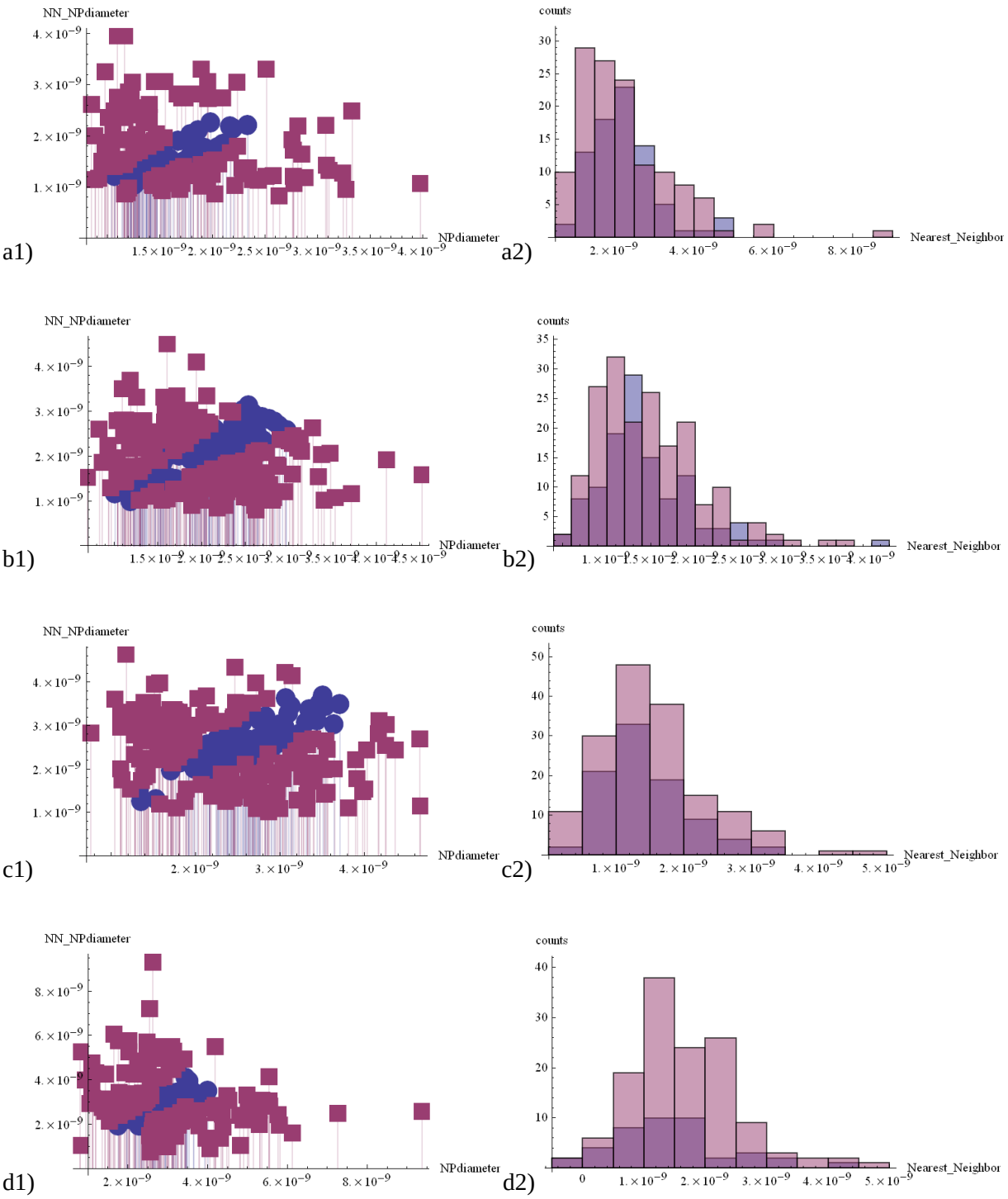

Figure S 5. a1)-d1) correlation between NP diameter and diameter of the corresponding NN NP for sample A-D. a2)-d2) NN distance distribution for sample A-D. Blue: NPs with diameter less than 20% different from the one of the corresponding NN NP. Move: NPs with diameter more than 20% different from the one of the corresponding NN NP.

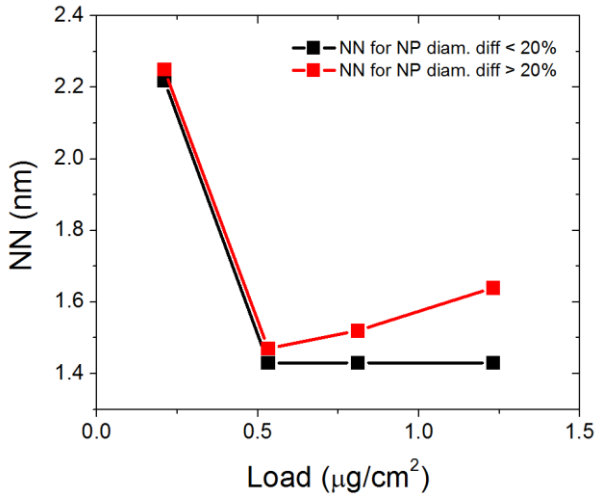

Figure S 6. evolution with the NP load of the NN distance of two NP groups: (black) NPs with diameter less than 20% different from the one of the corresponding NN NP, (red) NPs with diameter more than 20% different from the one of the corresponding NN NP

3 Observations regarding the NPs shape

The experimental data discussed in the film growth section seem to drive to a very interesting conclusion: during film growth (landing and coalescence) these Au NPs should have a spherical shape. Indeed, a very striking feature that it is noticed in the TEM images presented in the results section is the very good circularity of the Au NPs in any of the conditions discussed there. By analyzing the shape of the NPs in terms of their circularity and aspect ratio, defined as:

$$circularity = 4\pi \frac{area}{perimeter^2} \quad \text{(1 for circle, 0 for line)} \qquad \text{(S19)}$$

$$AspectRatio = \frac{MajorAxis}{MinorAxis} \quad \text{(1 for circle, } \infty \text{ for line)} \qquad \text{(S20)}$$

it is possible to realize that, in spite of the intense coalescence taking place as higher loads are approached, the NPs maintain their circularity and aspect ratio almost unchanged as shown in

Figure S 7. Histograms of the circularity and aspect ratio together with their correlation plots against the NPs area are shown in Figure S 8-Figure S 11 for the 4 samples. The vast majority of NPs in samples A-C have circularity in the range 0.9-1.0 and aspect ratio in the range 1.0-1.2. Sample D have circularity and aspect ratio distributions with longer tails than the other samples but still the vast majority of particles fall in the above mentioned ranges. This peculiar behavior is particularly interesting and unique to the case of such very small Au NPs. Materials other than Au, in the same high density/load conditions behave completely differently, either coalescing and creating islands with irregular shapes or simply by creating large agglomerates of single particles. The former behaviour has been observed for example using Pt NPs as shown in the low and high load TEM images in Figure S 12, while the latter has been found when using Si (Figure S 13) or Ni(Figure S 14). Furthermore, we do know that the as produced NPs by the cluster beam generator, that in TEM plan view images appear circle-like, are spherical or quasi-spherical even when they are as large as 10 nm in diameter, as found from ourselves (Figure S 15) and others [2]. The reason we stress this point is that we believe that shape parameters like circularity and aspect ratio could actually also be indirect indicators for sphericity given that the film growth analysis, as mentioned in the manuscript, do suggest a 3D growth of the NPs in the coalescence regime. Indeed, from the literature regarding the kinetics of Au film growth someone can easily realize that flattened Au NPs are always characterized by having irregular shapes, clearly and unmistakably far from being circular [3,4 ,5 ,6]. The question then is, could the circular shape seen in TEM plane view, be used as a proof of sphericity? We argue that the answer to this question is yes, at least for such small Au NPs. The reason is that our results seem to support a very intense coalescence with 3D growth taking place in our samples but still the shape indicators are not affected by it, which we interpret concluding that when such small Au NPs coalesce they

completely redistribute their Au atoms in order to create a new NP with the lowest possible configurational energy, be it electronic or geometrical. Apparently it is only when the coalescing Au NPs are quite "large" that we start observing pronounced tails in the distributions of the shape indicators, as in sample D, marking probably in such way the loss of sphericity and creation of flattened clusters/islands as so many authors reported in the literature regarding Au film growth.

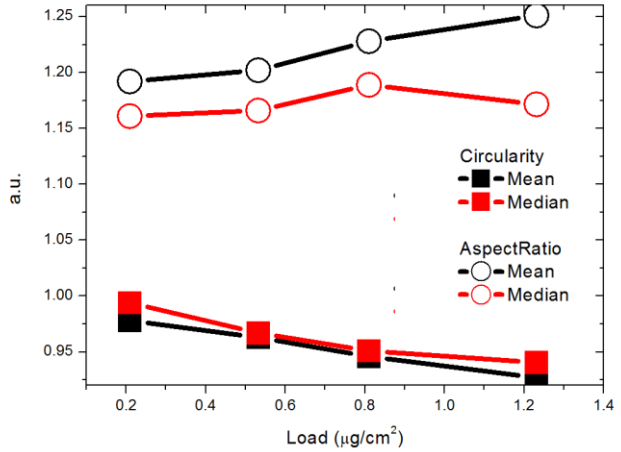

Figure S 7. AspectRatio and Circulaty as a function of the Au load. No big changes are observed in these shape factors.

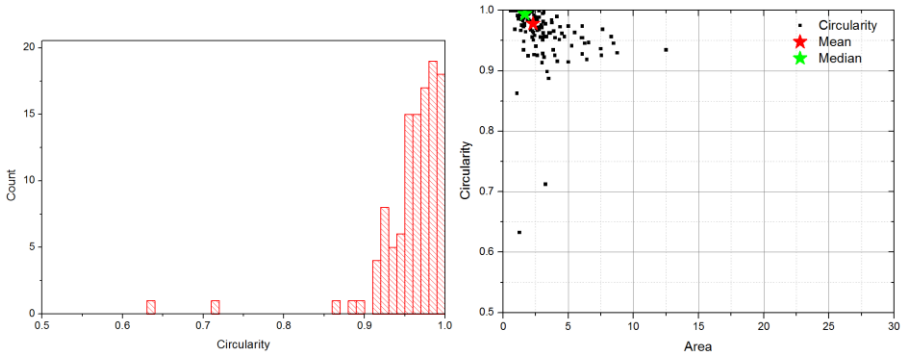

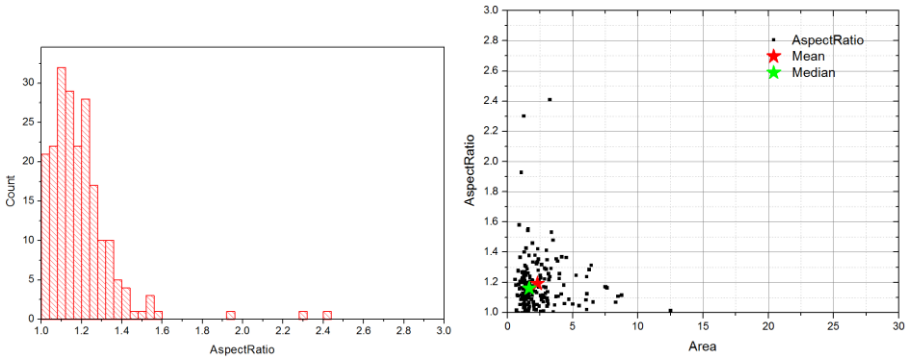

Figure S 8. Circularity and AspectRatio for sample A

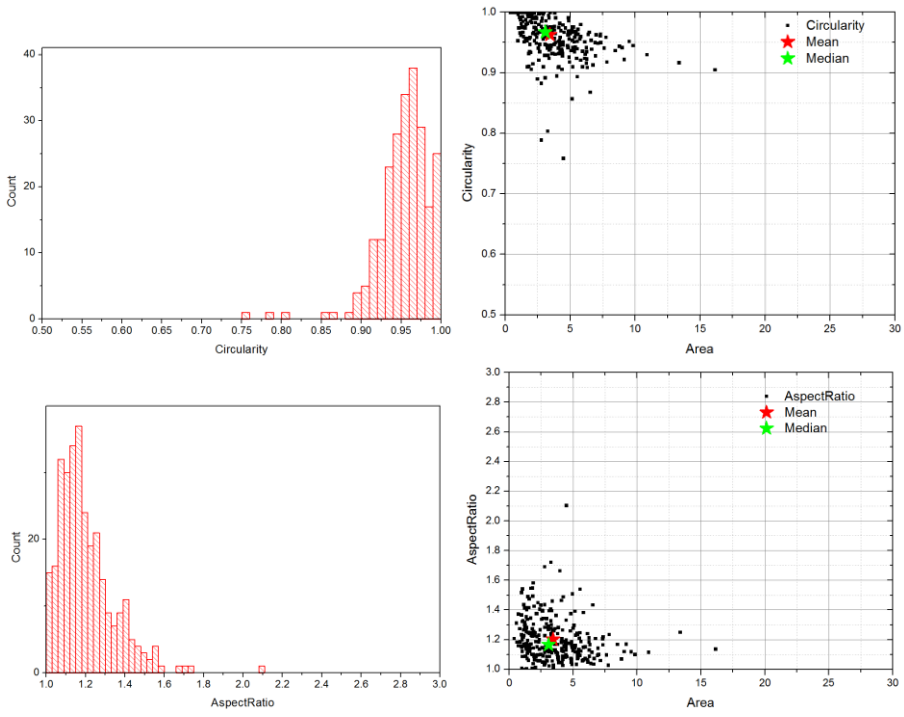

Figure S 9. Circularity and AspectRatio for sample B

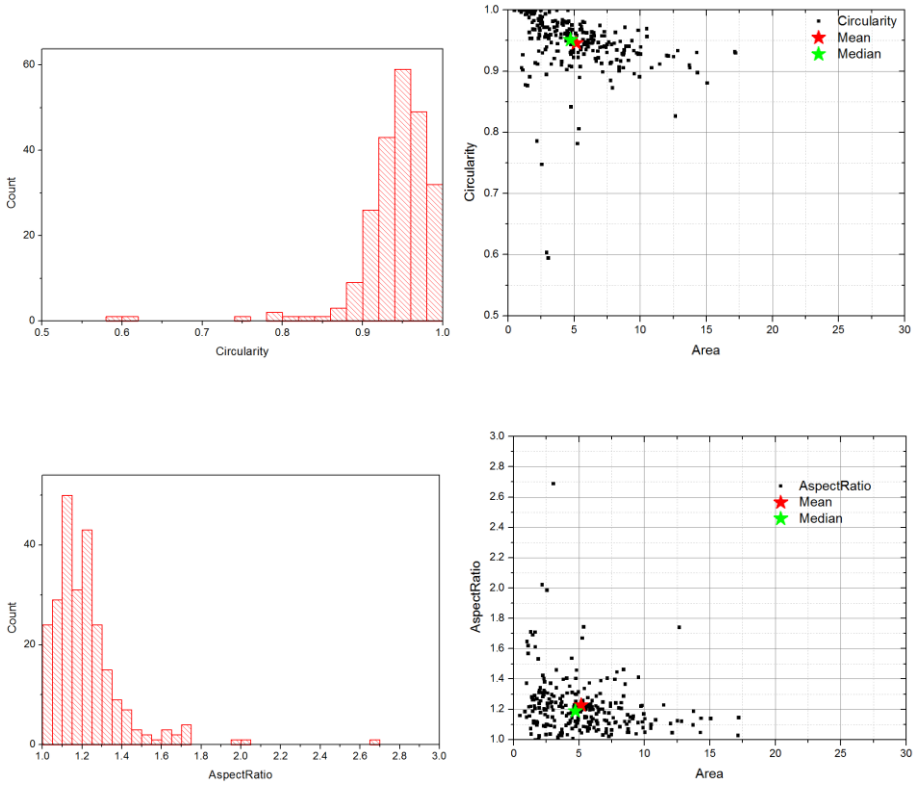

Figure S 10. Circularity and AspectRatio for sample C

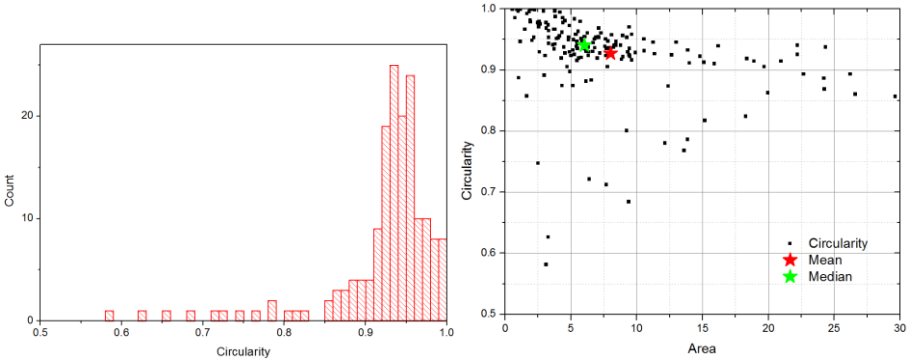

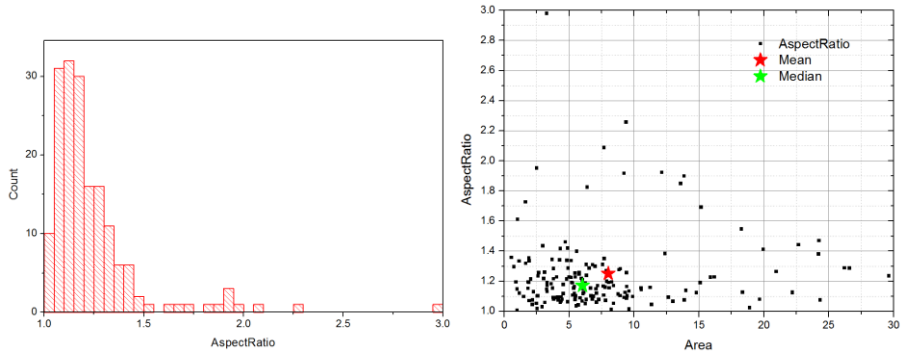

Figure S 11. Circularity and AspectRatio for sample D

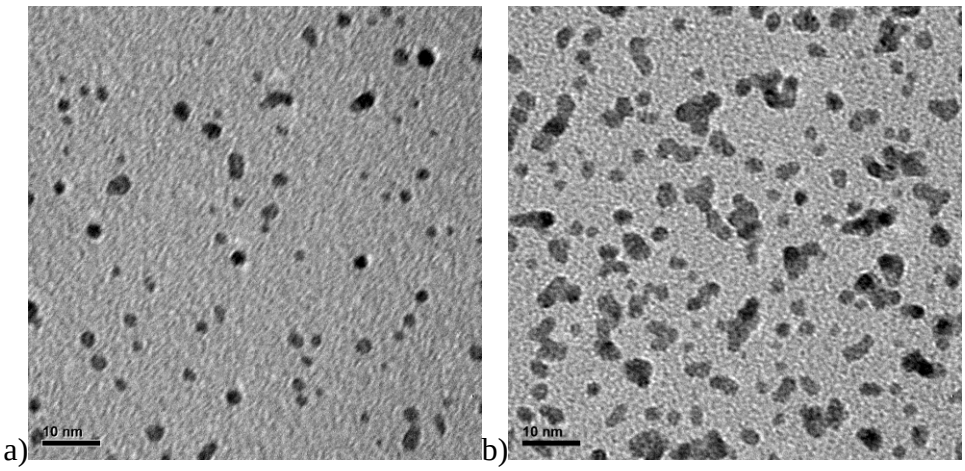

a) b)

Figure S 12. Pt NPs at a)low and b)high load

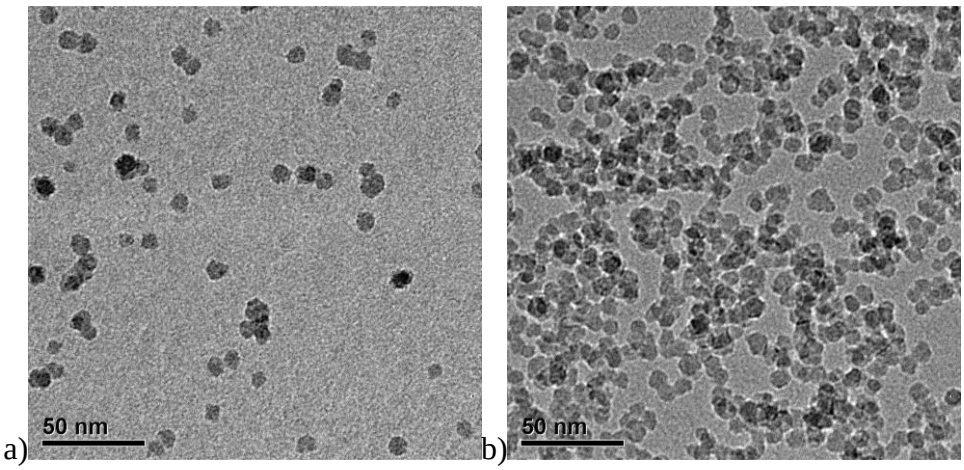

a) b)

Figure S 13. Si NPs at a)low and b)high load

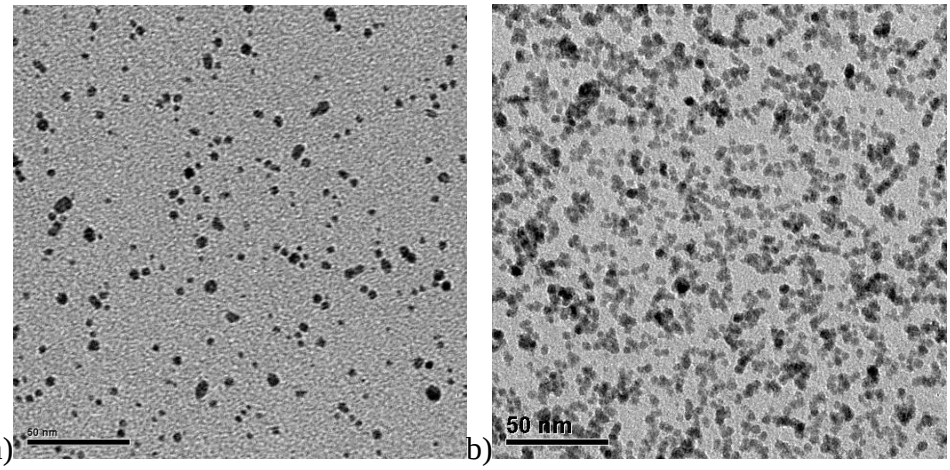

a) b)

Figure S 14. Ni NPs at a)low and b)high load

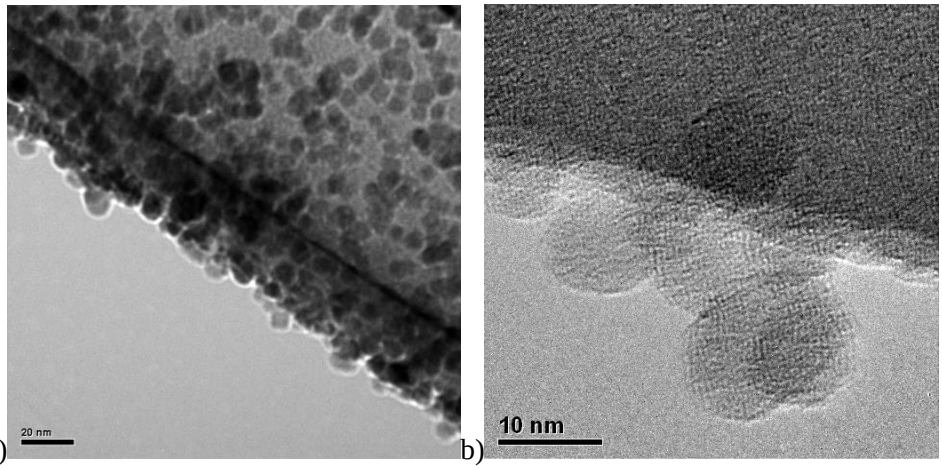

a) b)

Figure S 15. TEM images showing a)Ni NPs and b)Si NPs on a broken portion of a carbon grid, allowing us to observe the particles as they protrude outward from the grid's surface. It is quite clear how even such large particles generated with the cluster beam are quasi-spherical.

4 Magic Numbers

The way matter behaves as we move from atoms to ideally infinite crystals, a field that today could be called nanocluster physics, has been the subject of intense investigations in the last decades with several seminal works representing milestones in the understanding of the link between atomic properties of isolated atoms and collective properties of atoms in bulk crystals. Since the seminal work of Knight et al. in 1984 [7] it became clear that electronic and

geometrical characteristics of nanoclusters govern the intrinsic stability of the cluster itself which means that only clusters with a specific, **magic number, of atoms** may be much more stable than the cluster obtained by the addition or removal of 1 atom. Generally, the properties of **very small clusters** tend to be dominated by their electronic characteristics with the experimental data being explained extremely well by the so called Jellium model [7,8], and subsequent modifications [9]. In this model the valence electrons from each atom of the cluster are imagined free from the atom itself but under the influence of a potential well generated by the positively charged ionic cores whose spatial configuration is irrelevant in the spherical Jellium model (that is capable to explain only magic numbers of clusters from the group I elements) while is taken into consideration in the modified Jellium model (that allows explaining the fine structure of experimental data and the magic numbers of clusters from elements of groups other than group I). In such a way, this model describes a superatom, where electronic shell closing correspond to the experimentally observed magic number configurations, For reviews on this subject refer to [10,11]. On the other hand, in **large clusters** the geometric arrangements of the atoms into one of the possible polyhedra dominates over their collective electronic configuration and so electronic shell closings are replaced by geometric shell closings in explaining the experimentally observed magic number configurations. For a review on this matter refer to [12]. The boundary between these two distinct regimes has been identified to be at around 1600 atoms for Na nanoclusters [13] but could be very different for other metals.

The production of nanoclusters that are particularly stable has a tremendous technological importance. In fields like catalysis or drug delivery, in which intense research is ongoing since several decades now and that with the advent of nanotechnology is expected to further increase

in the near future, the key component is generally nanoclusters that promote certain chemical reactions to occur ideally without being permanetly altered by the process itself.

4.1 Detailed analysis concerning Au magic numbers

According to the Jellium model, electronic shell closures should take place when the number of atoms N in the cluster is equal to one of the following magic numbers: N=2, 8, 20, 40, 58, 92, 138, 190, 254, 338, 438, 546, 676, 832, etc [14]. This model applies very well to the elements of group I, as Na in the above reference. Apparently, as we move down the periodic table toward the heavier elements of higher groups, the above rule doesn't seem to hold exactly, at least not for Au in the transition metals. The literature on Au magic numbers, spanning more than 3 decades, is quite rich but also confusing and unclear to a point that asking the questions "at which point does the electronic shell closure give way to the geometric shell closure for Au clusters?" seem not the right question to ask as an answer does not seem to be available yet. What is clear is that the geometric shell closing seem to compete with the electronic shell closing and for this reason Au nanoclusters made of as little as few tens of atoms, have magic numbers that may also be related to the shell closing of regular polyhedra like tetrahedron, octahedron, decahedron, dodecahedron, icosahedron, etc [12]. Some of these polyhedra don't posses enough symmetry to grow into a bulk crystal, due to the strain that the structure would be facing [12], so they may be observed only at the nanoscale. Back in 1985, Katakuse et al. [15] investigating the mass distribution of Au clusters generated by Xe ions bombardment reported results supporting the existence of the Au magic numbers 2, 8, 20, 34, 58, 92, 138, 200, etc, in very good agreement with the sequence found just a year before by Knight et al. [7] for Na. Those results for Au were later confirmed by: Robin et al. [16] and Keki et al. [17] using a similar experimental approach, Wu et al. [18] using electroporation and Larsen et al. [19] using density functional theory (DFT).

Theoretical and experimental results highlighted though that also geometric shell closing could give rise to very stable Au structures, although for some of the structures there is still some ambiguity. One of the first references on this matter is the work from Phillips back in 1986 [20]. A decade later, Koga et al [21] using a cluster beam generator very similar to ours were able to identify the Au magic number 13 and also to establish, using in situ grazing incidence x-ray diffraction that such a cluster had icosahedral symmetry and diameter of 0.58 nm. They also argued that the next geometric closures for the icosahedron would be at 55, 147, 309 giving Au clusters with diameters of 1.17 nm, 1.74 nm, 2.32 nm respectively [22]. It is worth noticing that a further reason for the particular stability of the Au clusters following the above sequence is actually that several polyhedra have geometrical shell closures at those particular magic numbers, like the icosahedron, cuboctahedron, twinned cuboctahedron, truncated decahedron, etc [12], confirmed experimentally by Li et al [23] for the case of the Au magic number 309 produced by a cluster beam generator. In a second experiment just a couple of years later, Koga et al. [24] provided evidence of the existence of decahedral Au magic numbers following the sequence 7, 23, 54, 105, 181, 287,etc. A very stable structure is also the tetrahedron [25] which should follow the sequence 4, 10, 20, 35, 56, 84, 120, etc [12]. A characteristic example that has been confirmed is the case of the Au magic number 20 [26,27,28] and recently Wang et al [29] also provided an estimation of its size to be around 1 nm. Interestingly also a quasi-tetrahedral Au cluster with 40 atoms has recently been observed [30].What appears to be clear from recent theoretical studies, taking advantage of the increased computational power offered by todays workstations, is that for a given number of Au atoms it is difficult to establish a relation between theoretical ground-state structures and experimental results, since in many cases the structure of clusters is determined by the kinetics of the growing process rather than by the energetic. What it is clear

though is that in the realm of the very small Au clusters with few tens or hundreds atoms, the addition of 1 atom to the cluster induces a complete rearrangement of the cluster itself and most of the times Au_N has a different geometry from Au_{N+1} [31]. Only larger clusters with several hundred atoms seem to prefer the geometries with quasi-spherical symmetry which prelude to the transition toward more bulk-like characteristics of the clusters. Apparently, according to Kleis et al [32], bulk surface properties for Au are reached at around 560 atoms (2.7 nm).

4.2 Experimental relation between Au NP diameter and the NP volume in atoms

In the literature there are several works that provide for a given Au magic number the diameter of the corresponding NP. It is obvious that the NP volume in atoms should scale approximately with the third power of the NP diameter. The quest of such a relation is particularly important in our case because 1) would allow us to provide a reasonable estimation of the NP size in atoms for the NPs observed in the samples fabricated in this work and 2) would also make it possible to try to identify candidate magic numbers according to the existing literature. To this purpose, six works from the vast literature on Au magic numbers were selected, covering the range of magic number clusters made of 13-40000 atoms and the result presented in Figure S 16. Having such a relation at hand it was then possible to produce volume vs diameter graphs of Au clusters of several works, estimating where needed the missing parameter of the two as shown in Figure S 17a (for experimental and theoretical works) or as shown in Figure S 17b (for major polyhedra).

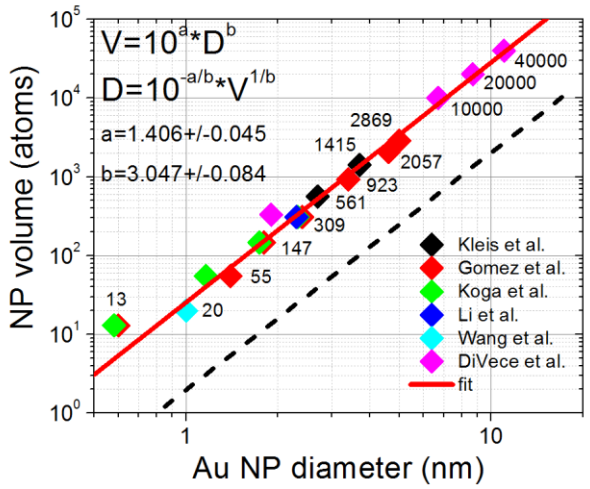

Figure S 16. data concerning volume and diameter of particularly stable Au clusters (magic numbers) retrieved from experimental works providing volume and diameter of magic clusters [33,34,35,36,37,38]. The best fit has been carried out in the range 20-40000 atoms as the Au cluster with 13 atoms seem to represent a special case that deviates quite a lot from the rest. In the fitted region the data seem to be in very good agreement with a power-like of order 3 dependence of the volume in atoms from the diameter as expected; the black dashed line represents a guide to the eye for the ideal 3rd power behavior. The fitting parameters provided in the graph allow calculating the volume in atoms for a given diameter of the Au cluster and viceversa by using the equations provided.

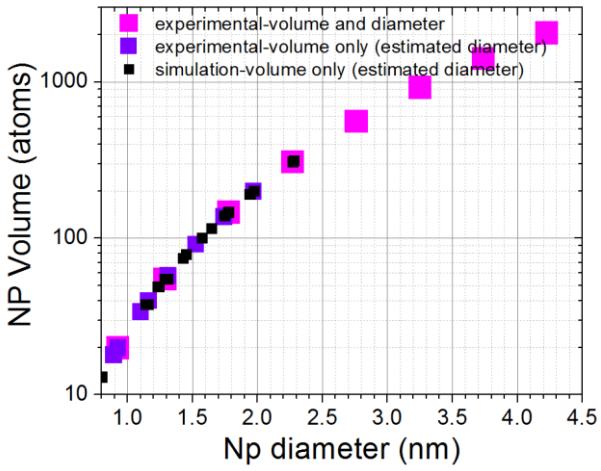

a)

b)

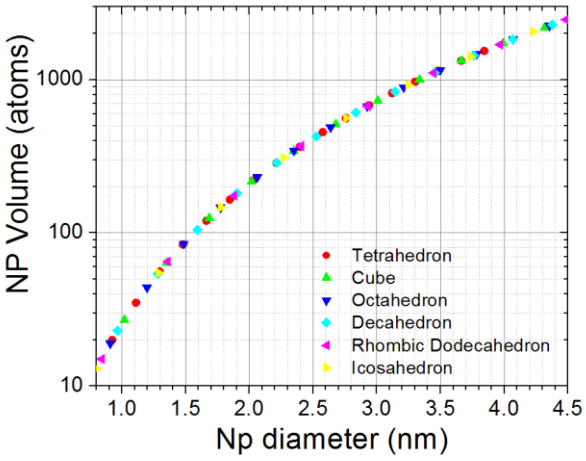

Figure S 17. a) summary of the data concerning volume and diameter of particularly stable Au clusters (magic numbers) retrieved from the literature from: experimental works providing volume and diameter of magic clusters [33,34,35,36,37,38], experimental works providing only the volume of the magic clusters [39,40,41], theoretical works providing only the volume of the magic clusters [42,43]. b) summary of the data concerning volume and diameter of particularly of major relevant polyhedra [44]

4.3 Peak analysis of NP size distributions

In this section we will use the volume vs diameter data developed here above to break down, when possible, the NP diameter distribution of each sample in potential Au magic numbers. An interesting feature that can be easily observed in the NP diameter distributions is that, by using a relatively large bin sizes, it is possible to highlight the presence of two distinct broad NP populations in the 4 samples, A-D: population 1 centered roughly in the 1-2 nm range and a population 2 in the range 2-3.5 nm. In particular it would seem that in the landing regime population 1 is dominating over 2 but as we move through B, C and D, population 2 becomes the dominating one at expenses of population 1, as shown in Figure S 18. By further decreasing the bin size considered, it is actually possible to reveal the fine structure of these two populations and identify potential magic numbers, which will be the subject of the next paragraphs. We

should remark that decreasing the bin size presents the danger to create artifacts that have nothing to do with real peaks related to a NP magic number. For this reason, in order to validate a certain peak we always check that it is a real stable feature of the distribution independent from the bin size chosen. This approach will become clear here below.

4.3.1 Short deposition sample

In the very early stages of NP deposition, see Figure S 19b, the NP diameter distribution shows two very clear peaks at around 0.95 nm and 1.25 nm that represent the dominating NP populations. Although the statistics is relatively poor, there are also other minor features that, in light of the discussion regarding the other samples, is worth investigating. In order to reliably define which features are real "peaks" and which are potential artifacts, the bin size of the distribution has been swept in the range 0.05-0.12 nm and at each step the position of every feature that could resemble a peak recorded. In this way Figure S 19a was generated where the grayed zones represent a guide to eye for those peaks that we attributed to real features of the distribution and can also be used to define a sort of standard error that could be attributed to the identified peak. The diameters of the identified peak are then used to calculate the corresponding volume in atoms of the cluster, using the relation obtained in Figure S 16, and the (x,y) data obtained in such a way are superimposed on Figure S 17a and Figure S 17b to allow identification to known Au magic structures, as shown for this case in Figure S 19c and Figure S 19d. While the 1.25 nm peak is in very good agreement with Au_{55}, the 0.95 nm peak could represent Au_{20} but due to the resolution limit of the TEM which makes such NPs appear quite blurry we cannot exclude that this peak could be related to Au_{13} instead. The other NPs observed in this phase of the deposition occur much less compared to the other two just discussed but surprisingly do fall near major magic numbers related to shell closures: Au_{147} and Au_{307} with

diameter around 1.7 nm and 2.3 nm respectively. An interesting feature of the distribution is the faint peak at around 1.5 nm which could be identified as Au_{92}. Finally we should note that the NPs in the bin around 1.9-2.0 nm and 2.5-2.6 nm, although the statistics in this case is extremely poor, also correspond to recurrent Au clusters as will also become clear from the analysis of next samples. The former is attributed to either Au_{200} or to the geometrical shell closure of the decahedron at Au_{181} occuring at 1.9 nm, while the latter is compatible with the geometrical shell closure of the decahedron at Au_{428} .

4.3.2 Sample A

The analysis of the fine structure of the NP distribution concerning sample A is shown in Figure S 20. Most of the peaks are the same with those observed during the short deposition discussed previously, i.e $Au_{20}(Au_{13})$, Au_{55}, Au_{92}, Au_{147}, $Au_{181}(Au_{200})$, Au_{307}, Au_{428} with the addition of a faint peak at 2.75 nm that matches perfectly the magic number Au_{561}. This analysis clearly justifies the fact that sample A is in the landing regime: its peaks match very well those related to the NPs generated by the cluster beam (short deposition) and from the presence of the new peak related to Au_{561} we can get a quick confirmation supporting the argument mentioned in the film growth kinetics section that in sample A together with the dominating landing process there is also a minor coalescence taking place. We should remark here a very interesting result, that is also the key point of this work, arising from this analysis: **the coalescence at substrate level of the NPs generated by the cluster beam have driven to the appearance of 1 new peak that apparently corresponds to a cluster that matches very well a magic number**. In other words kinetics processes at substrate level drove to the formation of a magic number through the coalescence on the substrate of two or more preexisting NPs.

4.3.3 Sample B

Regarding sample B, shown in Figure S 21, the identified peaks correspond to structures also seen in sample A, i.e. Au_{55}, Au_{92}, Au_{147}, Au_{181}(Au_{200}), Au_{307}, Au_{428}, Au_{561}, with the addition of two faint peaks on the tail of the distribution at 3.15 nm and 3.35 nm that we attribute to the magic number Au_{923} (electronic shell closure) and Au_{1111} (decahedron geometrical shell closure) respectively. Although this identification may seem quite arbitrary at this point, we will see that these two peaks are stable features of samples C and D as well and the above identification seems the most appropriate. We should note that in this case we didn't observe a stable peak around 0.9 nm (identified as Au_{20} or Au_{13}), as we did for sample A. We will see that this peak will either be absent or be barely distinguishable also in sample C and D indicating the fact that the small clusters, which are also the most mobile at substrate level, are probably those that contribute the most to processes 1-2 or 1-3 in the coalescence regime (samples B-D) thus driving to a very high consumption rate of such clusters and explaining the lack of them from the NP distributions.

4.3.4 Sample C

The analysis regarding sample C is shown in Figure S 22. Some features are the same as sample B, i.e. Au_{92}, Au_{147}, Au_{307}, Au_{428}, Au_{561}, Au_{923}, Au_{1111} with the addition of a very intense peak next to Au_{561} matching quite well Au_{609} (decahedron geometrical shell closure) and two faint peaks at 4.0 and 4.25 nm identified as Au_{1823} (decahedron geometrical shell closure) and Au_{2057} (electronic shell closure). In this sample cannot be distinguished any peak in correspondence of Au_{20} and Au_{55}, in agreement with the arguments presented here above regarding sample B.

4.3.5 Sample D

Regarding sample D, shown in Figure S 23, most of the features are the same with sample C i.e. Au_{55}, Au_{92}, Au_{147}, Au_{181}(Au_{200}), Au_{307}, Au_{561}, Au_{923}, Au_{1111}, Au_{1823}, Au_{2057}; on the tail of the distribution there are some features that could represent peaks but the statistics is too poor to safely identify such structures.

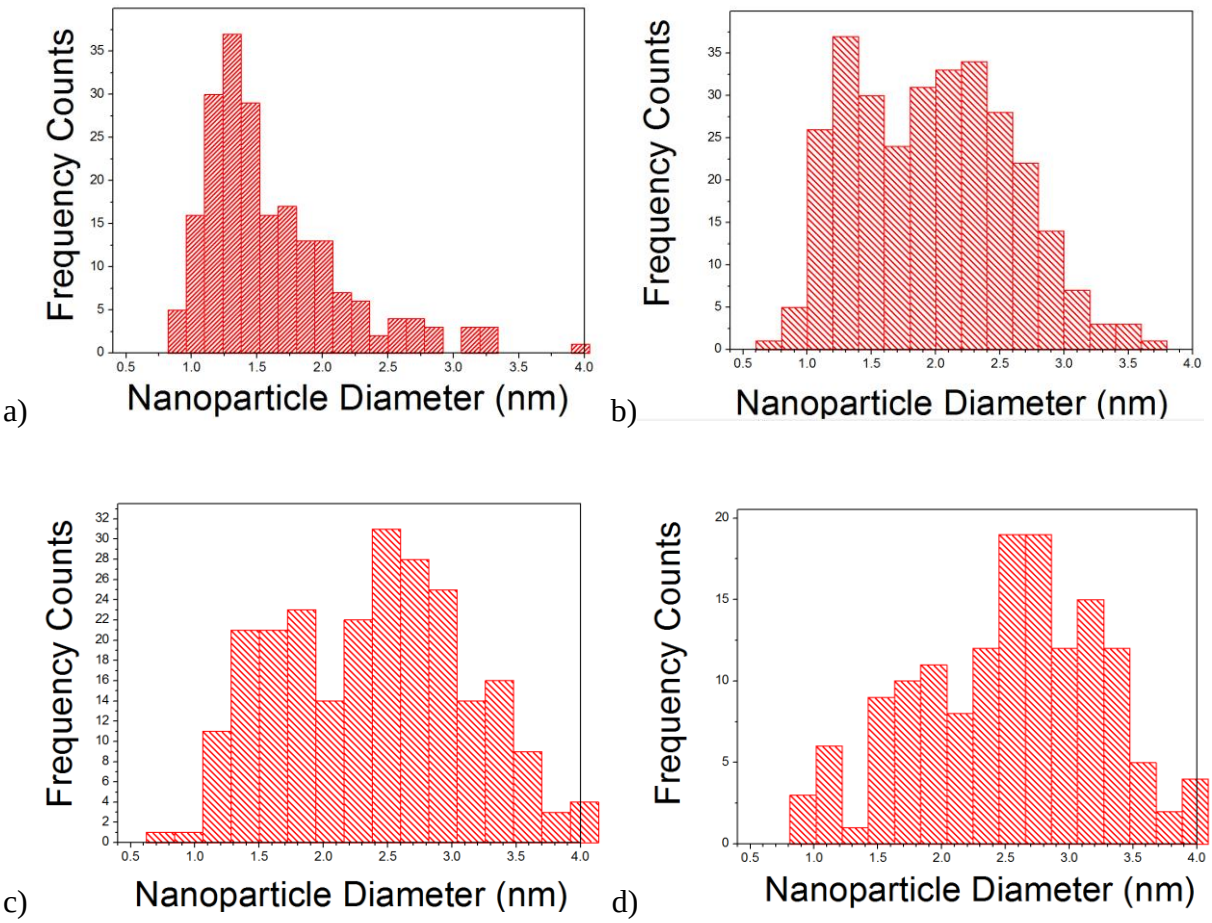

Figure S 18. NP diameter distribution for sample a) A, b) B, c) C and d) D.

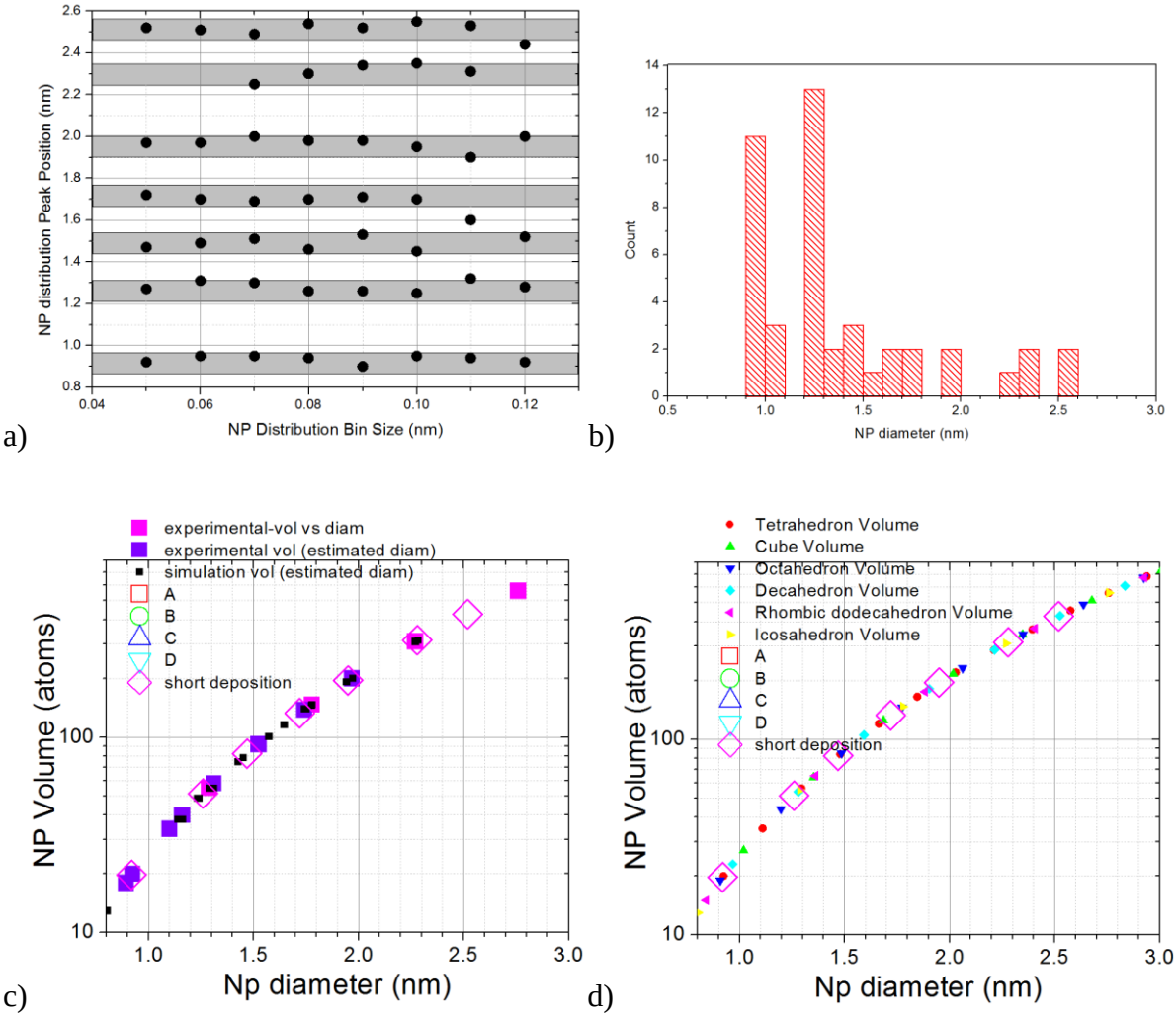

Figure S 19. short deposition

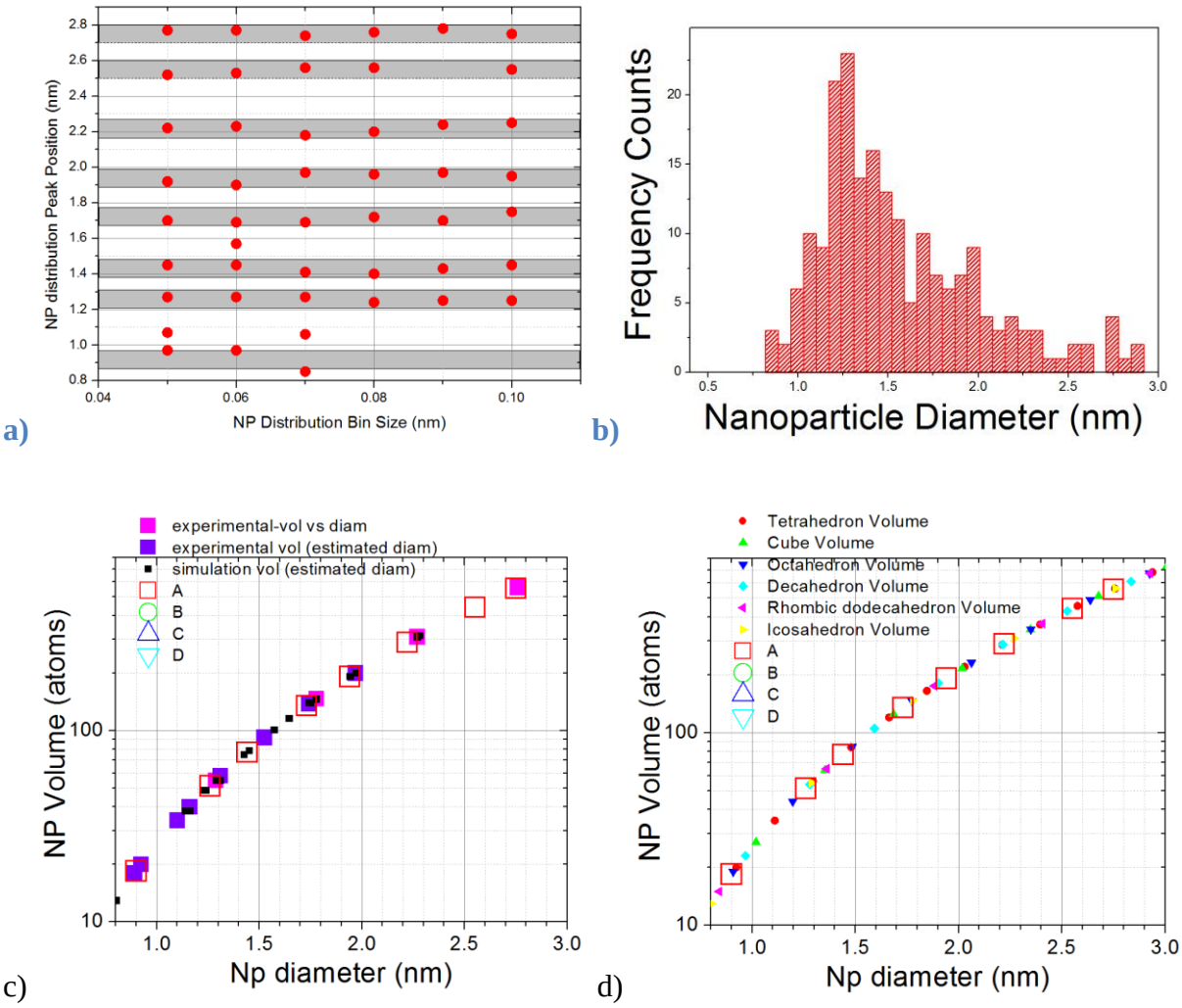

Figure S 20. Sample A

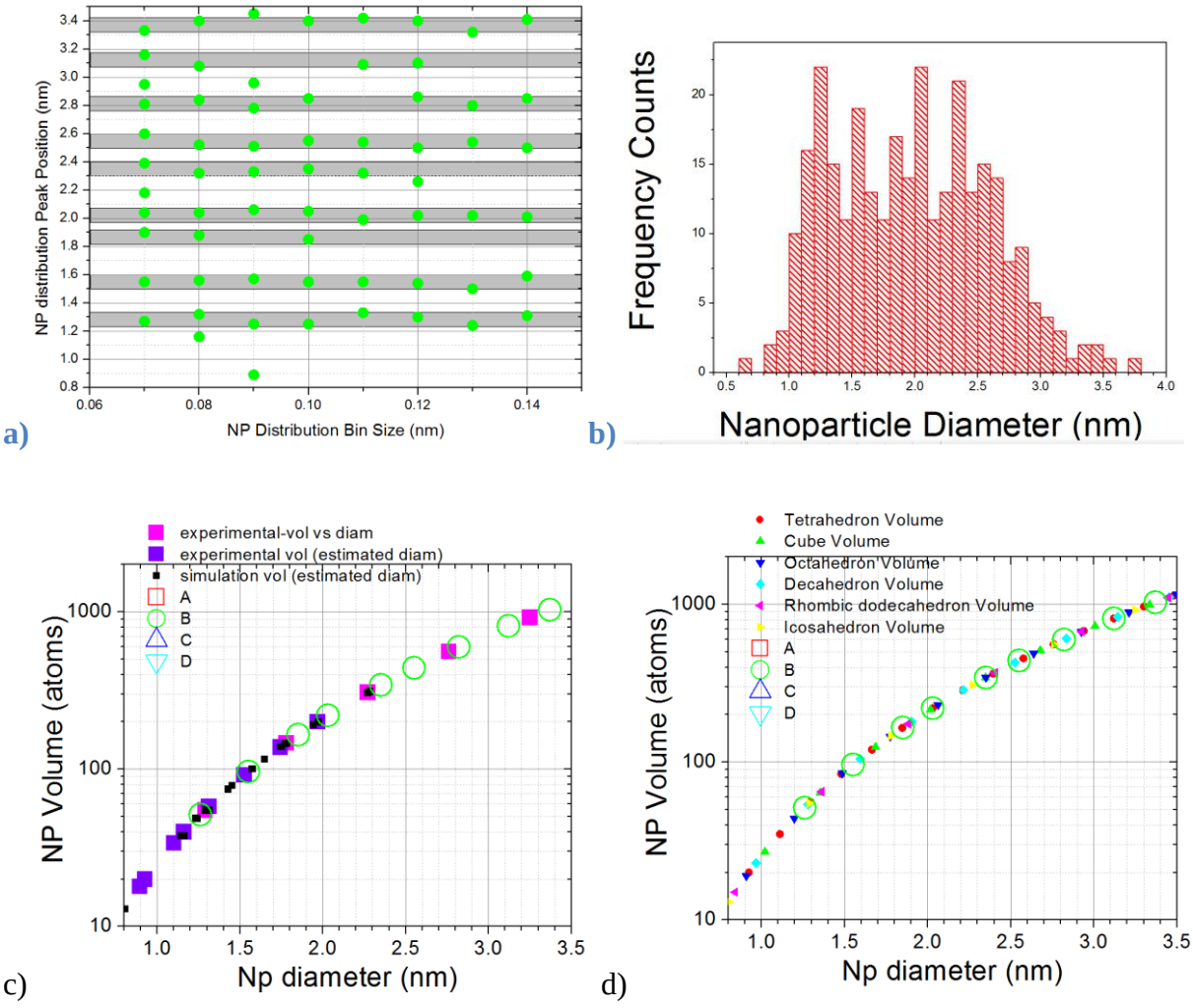

Figure S 21. Sample B

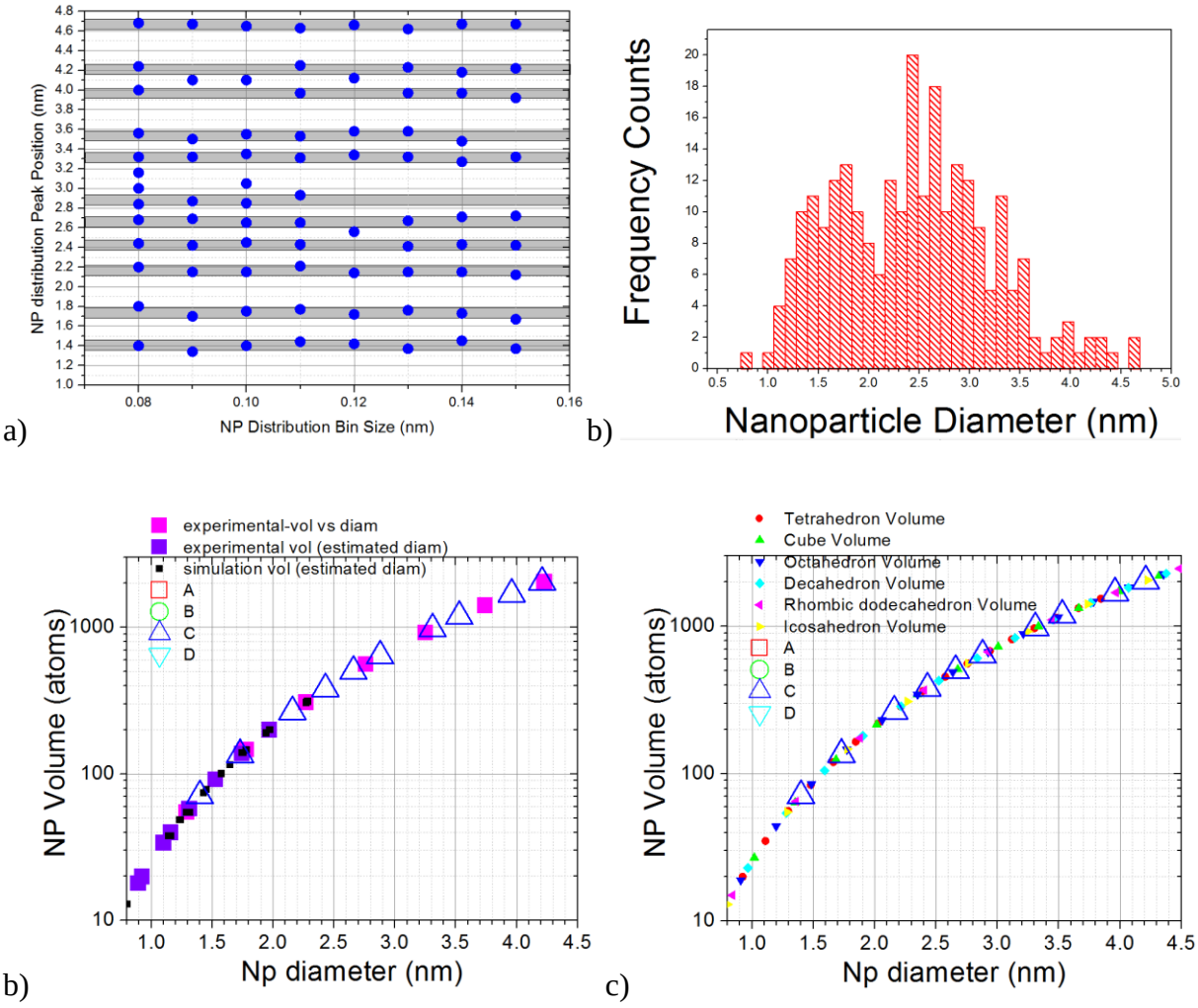

Figure S 22. Sample C

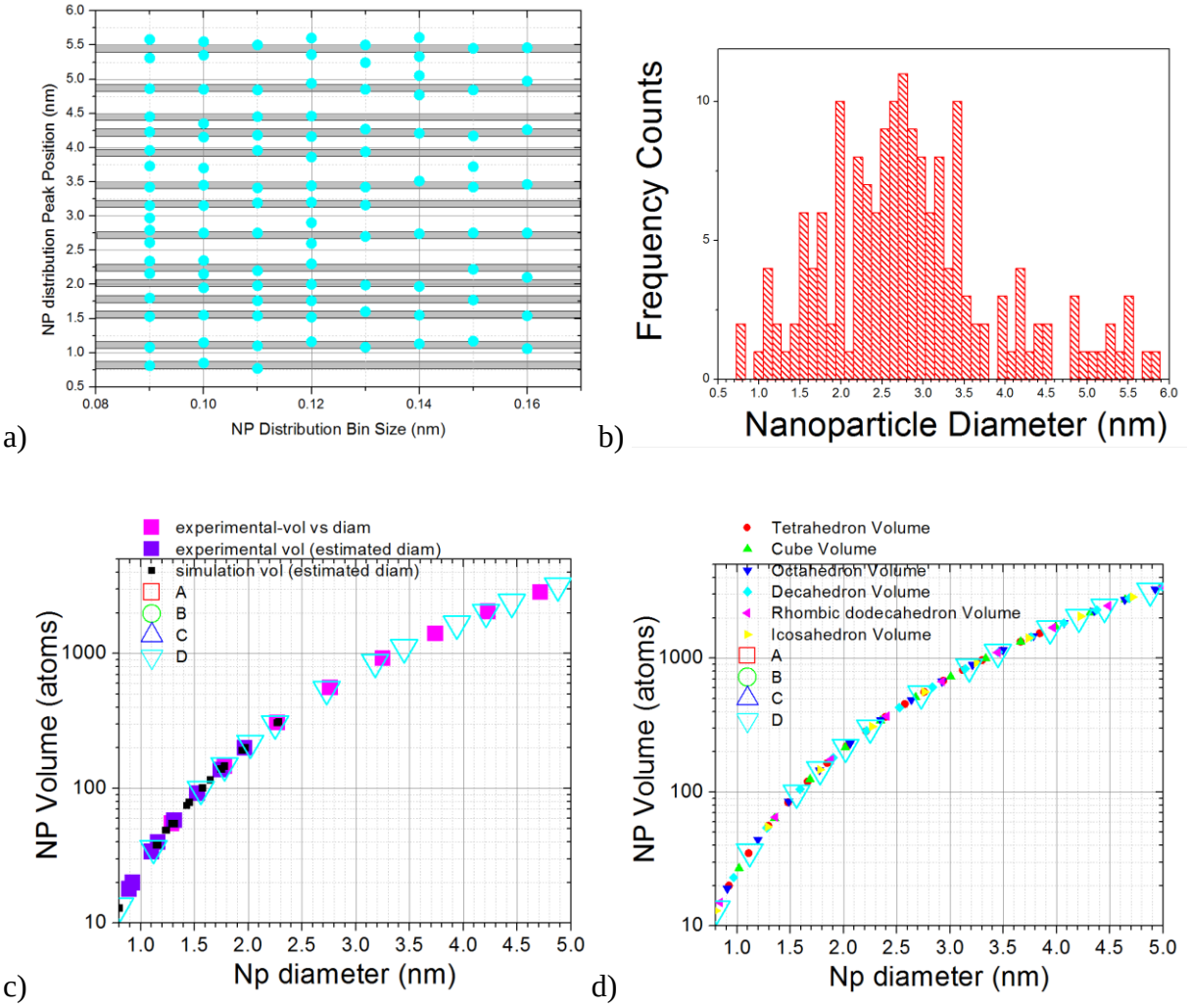

Figure S 23. Sample D

5 References

[1] GIAS, Geological Image Analysis Software, available online (free) at www.geoanalysis.org.

[2] D. B. Pedersen and S. Wang, J. Phys. Chem. C 2012, 116, 3258−3265

[3] N Vandamme, E Janssens, F Vanhoutte, P Lievens1 and C VanHaesendonck, J. Phys.: Condens. Matter 15 (2003) S2983–S2999

[4] Ignacio López Salido, PhD dissertation, Konstanz University (2007), available online at http://www.ub.uni-konstanz.de/kops/volltexte/2007/2707/

[5] T. Okazawa, M. Kohyama, Y. Kido, Surface Science 600 (2006) 4430–4437

[6] A. Rota, A. Martinez-Gil, G. Agnus, E. Moyen, T. Maroutian, B. Bartenlian. Me´gy, M. Hanbu¨cken, P. Beauvillain, Surface Science 600 (2006) 1207–1212

[7] W, D. Knight, K. Clemenger, W. A. de Heer, W. A. Saunders, M. Y. Chou, and M. L. Cohen, Phys. Rev. Lett. 52, 2141 (1984)

[8] W. Ekardt, Phys Rev B, 31, 10, 6360 (1984)

[9] K. Clemenger, Phys Rev B, 32, 2, 1359 (1985)

[10] M. Brack, Rev Mod Phys, 65, 3, 677 (1993)

[11] Walt A. de Heer, Rev Mod Phys, 65, 3, 611 (1993)

[12] T.P. Martin, Physics Reports, 273, 199 (1996)

[13] Clemenger, K., (1991),Phys. Rev. 8 44, 12991

[14] S.M. Reimann 1, M. Brack 1, Klavs Hansen, Z. Phys. D 28, 235-245 (1993)

[15] I. Katakuse, T. Ichihara, Y. Fujita, T. Matsuo, T. Sakurai, H. Matsuda, International Journal of Mass Spectrometry and Ion Processes, 67 (1985) 229-236

[16] I. Rabin, C. Jackschath, and W. Schulze, Z. Phys. D - Atoms, Molecules and Clusters 19, 153-155 (1991)

[17] Sándor Kéki, Lajos Nagy, György Deák, and Miklós Zsuga, J Am Soc Mass Spectrom 2004, 15, 1455–1461

[18] Sixin Wu, Hongxia Zeng, and Zoltan A. Schelly, J. Phys. Chem. B, Vol. 109, No. 40, 2005

[19] A. H. Larsen, J. Kleis, K. S. Thygesen, J. K. Nørskov, and K. W. Jacobsen, Physical Review B 84, 245429 (2011)

[20] J. C. PHILLIPS, chem. Rev. 1980. 88. 619-634

[21] Kenji Koga and Harutoshi Takeo, Review of Scientific Instruments 67, 4092 (1996);

[22] J.C. Ruiz G´omez and L. Rinc´on, Revista Mexicana DE F´isica S 53 (7) 208–211

[23] Z. Y. Li, N. P. Young, M. Di Vece, S. Palomba, R. E. Palmer, A. L. Bleloch, B. C. Curley, R. L. Johnston, J. Jiang, J. Yuan, Nature, Vol 451, 3 January 2008

[24] Kenji Koga, Harutoshi Takeo, Takuji Ikeda and Ken-ichi Ohshima, Physical Review B Vol 57, No 7, (1998)

[25] S. M. Reimann, M. Koskinen and H. Ha¨kkinen, P. E. Lindelof, M. Manninen, Physical Review B Vol 56, No 19, 1997

[26] B. Soule´ de Bas, M.J. Ford*, M.B. Cortie, Journal of Molecular Structure (Theochem) 686 (2004) 193–205

[27] Philipp Gruene, David M. Rayner, Britta Redlich, Alexander F. G. van der Meer, Jonathan T. Lyon, Gerard Meijer, Andr´e Fielicke, Science 2008 Vol. 321 no. 5889 pp. 674-676

[28] Jun Li, Xi Li, Hua-Jin Zhai, Lai-Sheng Wang, Science 2003, Vol. 299 no. 5608 pp. 864-867

[29] Z. W. Wang and R. E. Palmer, Nanoscale, 2012, 4, 4947

[30] De-en Jiang, Michael Walter, Physical Review B 84, 193402 (2011)

[31] Kuo Bao, Stefan Goedecker, Kenji Koga, Frédéric Lançon, and Alexey Neelov, Physical Review B 79, 041405, 2009

[32] J. Kleis, J. Greeley, N. A. Romero, V. A. Morozov, H. Falsig, A. H. Larsen, J. Lu, J. J. Mortensen, M. Dułak, K. S. Thygesen, J. K. Nørskov, K. W. Jacobsen, Catal Lett (2011) 141:1067–1071

[33] M DiVece, N P. Young, Z Li, Y Chen, and R E. Palmer, Small 2006, 2, No. 11, 1270 – 1272

[34] Kenji Koga and Harutoshi Takeo, Review of Scientific Instruments 67, 4092 (1996);

[35] J.C. Ruiz G´omez and L. Rinc´on, Revista Mexicana DE F´isica S 53 (7) 208–211

[36] Jun Li, Xi Li, Hua-Jin Zhai, Lai-Sheng Wang, Science 2003, Vol. 299 no. 5608 pp. 864-867

[37] Z. W. Wang and R. E. Palmer, Nanoscale, 2012, 4, 4947

[38] J. Kleis, J. Greeley, N. A. Romero, V. A. Morozov, H. Falsig, A. H. Larsen, J. Lu, J. J. Mortensen, M. Dułak, K. S. Thygesen, J. K. Nørskov, K. W. Jacobsen, Catal Lett (2011) 141:1067–1071

[39] I. Katakuse, T. Ichihara, Y. Fujita, T. Matsuo, T. Sakurai, H. Matsuda, International Journal of Mass Spectrometry and Ion Processes, 67 (1985) 229-236

[40] I. Rabin, C. Jackschath, and W. Schulze, Z. Phys. D - Atoms, Molecules and Clusters 19, 153-155 (1991)

[41] Sándor Kéki, Lajos Nagy, György Deák, and Miklós Zsuga, J Am Soc Mass Spectrom 2004, 15, 1455–1461

[42] A. H. Larsen, J. Kleis, K. S. Thygesen, J. K. Nørskov, and K. W. Jacobsen, Physical Review B 84, 245429 (2011)

[43] Kuo Bao, Stefan Goedecker, Kenji Koga, Frédéric Lançon, and Alexey Neelov, Physical Review B 79, 041405, 2009

[44] T.P. Martin, Physics Reports, 273, 199 (1996)